Hindawi
International Journal of Photoenergy
Volume 2019, Article ID 8982672, 8 pages
https://doi.org/10.1155/2019/8982672

Research Article

Atomic Layer Deposition of TiO_2 Nanocoatings on ZnO Nanowires for Improved Photocatalytic Stability

Emmeline Kao,[1,2] **Hyun Sung Park**,[1,2] **Xining Zang**,[1,2] **and Liwei Lin**[1,2]

[1]*Berkeley Sensor and Actuator Center, Berkeley, CA 94704, USA*
[2]*Mechanical Engineering, University of California Berkley, Berkeley, CA 94704, USA*

Correspondence should be addressed to Emmeline Kao; kao@berkeley.edu

Emmeline Kao and Hyun Sung Park contributed equally to this work.

Received 30 January 2019; Revised 20 March 2019; Accepted 28 March 2019; Published 9 May 2019

Guest Editor: Wei Wei

Copyright © 2019 Emmeline Kao et al. This is an open access article distributed under the Creative Commons Attribution License, which permits unrestricted use, distribution, and reproduction in any medium, provided the original work is properly cited.

Photocatalytic water splitting represents an emerging technology well positioned to satisfy the growing need for low-energy, low CO_2, economically viable hydrogen gas production. As such, stable, high-surface-area electrodes are increasingly being investigated as electrodes for the photochemical conversion of solar energy into hydrogen fuel. We present a titanium dioxide (TiO_2)/zinc oxide (ZnO) nanowire array using a hybrid hydrothermal/atomic layer deposition (ALD) for use as a solar-powered photoelectrochemical device. The nanowire array consists of single crystalline, wurtzite ZnO nanowires with a 40 nm ALD TiO_2 coating. By using a TiO_2 nanocoating on the high surface area-ZnO array, three advancements have been accomplished in this work: (1) high aspect ratio nanowires with TiO_2 for water splitting (over 8 μm), (2) improved stability over bare ZnO nanowires during photocatalysis, and (3) excellent onset voltage. As such, this process opens up new class of the micro/nanofabrication process for making efficient photocatalytic gas harvesting systems.

1. Introduction

It has been estimated that 37.7 Mt/yr of hydrogen gas (H_2) would be enough to replace all coal currently used in the United States [1]. However, steam reformation—the dominant method for producing H_2 today—involves burning methane with high-temperature steam to create H_2, producing carbon dioxide as a by-product ($CH_4 + H_2O$ (+ heat) $\longrightarrow$ $CO + 3H_2$). Other methods include electrolysis by solar cells, renewable liquid reformation, and fermentation; these are plagued by low solar-energy-to-water efficiency, low yields, and poor selectivity [2].

By contrast, photoelectrochemical (PEC) water splitting has the potential to passively convert solar energy into H_2 more effectively than electrolysis through the use of photovoltaics (PV). PEC water splitting is capable of higher yield and selectivity while producing zero carbon emissions. Utilizing photogenerated electron/hole pairs, the PEC process involves oxidizing water ($2H_2O + 4h^+ \longrightarrow 4H^+ + O_2$) and reducing the resulting H^+ ions ($4e^- + 4H^+ \longrightarrow 2H_2$) at the semiconductor/electrolyte interface while being submerged in an aqueous medium, as shown in Figure 1(a). In contrast to PV electrolysis, this process is theoretically more efficient since the PEC process experiences fewer losses to attain the required bias voltage [3]. Furthermore, water splitting scales easily with the area of the semiconducting material, making it ideal for large-scale, high-yield hydrogen harvesting. The selectivity of the PEC process is tunable with the band structure. That is, the bandgap, E_g, must be positioned correctly to allow for the reduction/oxidation reactions necessary to split water: conduction band should be above the reduction potential, and valence band should be below the oxidation potential. A Schottky barrier is formed at the photoelectrode-electrolyte interface. The system is designed such that minority carriers move into the electrolyte and begin reduction/oxidation of water. Majority carriers oxidize/reduce water at the counter electrode-electrolyte interface [4]. Figure 1(b) shows the energy band diagram for the photocatalytic system using an n-type, TiO_2 photoanode.

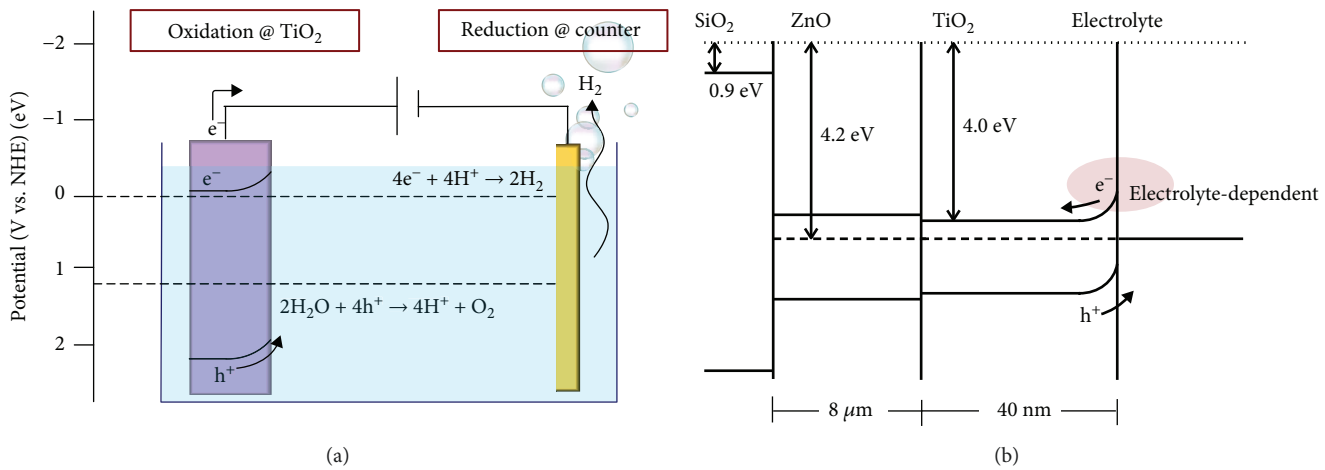

Figure 1: (a) Water splitting cell: incident light creates photogenerated electron-hole pairs. Given an appropriate band structure (straddling water reduction/oxidation potentials), holes and electrons will oxidize water at the photoanode and reduce resulting H^+ ions at the cathode, respectively. These reactions result in oxygen and hydrogen gas production. (b) Proposed band gap structure of TiO_2@ZnO: high-aspect ratio TiO_2 experiences charge separation at the electrolyte-TiO_2 interface, moving holes into the electrolyte and electrons into the single-crystalline ZnO nanowire.

Numerous studies have been aimed at achieving stable and efficient PEC systems using metal oxides responsive to solar spectrum, but they have suffered from three major drawbacks [5–7]: (1) low conversion efficiency due to recombination and quality of materials (for example, non-ideal crystallinity, where recombination can occur at grain boundaries), (2) high-onset voltages, and (3) poor material stability in the photocatalytic process [8]. Thus, much subsequent research has focused on either stabilization layers or texturization of the surface to increase conversion efficiencies in a highly oxidizing environment [9, 10]. By utilizing a hybrid hydrothermal/atomic layer deposition (ALD) ZnO/TiO_2 nanowire array, we are able to both stabilize the ZnO nanowire array through an ALD TiO_2 nanocoating while leveraging the architecture of the cell to improve performance. This hybrid hydrothermal/ALD texturization allows for conversion efficiency and improved onset voltage compared to untexturized, planar electrodes.

In the past, nanowires have shown three distinct improvements over untextured substrates: (1) enhanced light trapping due to light-concentrating properties of standing nanowires [11], (2) increased surface area, leading to increased active surface sites upon which water splitting can occur, and (3) reduced minority carrier distances, decreasing the rate of recombination and increasing charge separation [12].

TiO_2 is an intrinsically n-type semiconductor material with an energy band gap of 3.2 eV [13, 14]. Its band edge positions straddle water redox potentials, as shown in Figure 1(b). Moreover, TiO_2 is relatively inexpensive [15] and is used extensively in environmental photocatalysis [16], because of its high stability, even in a highly oxidizing aqueous environment [17]. However, the state-of-art TiO_2 usage as a PEC photoanode is plagued by lower photocurrent due to poor light absorption. Moreover, previous work on texturizing TiO_2 has not been able to produce high-aspect ratio TiO_2 nanowires due to undesirable compact layers at the bottom of the wire arrays [18]. In this work, we fabricate high-aspect ratio ZnO/TiO_2 nanowire arrays using a hybrid hydrothermal/ALD process. After growing the high-aspect ratio ZnO nanowires using the hydrothermal methods, we apply a uniform coating of TiO_2 by ALD. The resulting structures show excellent-onset voltage due to enhanced charge separation, which is induced by the geometry of our devices: by increasing the aspect ratio, we reduce travel distance of the minority carriers into the solution. Furthermore, TiO_2-coated ZnO nanoarrays show improved chemical stability over bare ZnO nanoarrays in aqueous solutions during photocatalysis.

2. Methods

A two-step hybrid process was used to fabricate the PEC water splitting devices, as shown in Figure 2. First, zinc oxide (ZnO) nanowires were fabricated by a hydrothermal process, serving as the template structure upon which the active material was deposited. Second, atomic layer deposition (ALD) was used to deposit 40 nm TiO_2. To fabricate ZnO, a seed solution of zinc acetate (Sigma) and ethanol were drop-casted onto n-type Si (100) wafers. The solution was left to form a quantum dot network on the surface of the Si wafers, rinsed with ethanol, and dried under nitrogen environment. The process was repeated 3 times to ensure adequate quantum dot formation. The wafer was annealed at 350°C for 30 min to ensure seed layer adhesion onto the wafer before being submerged in a growth solution containing zinc nitrate hexahydrate (Sigma), hexamethylenetetramine (Sigma), and ammonium hydroxide (Alfa Aesar) at 90°C for 8 hrs. The wafer was removed from the solution and cleaned with deionized water.

After the samples were dried, uniform deposition of TiO_2 over ZnO nanowires was performed using ALD, as

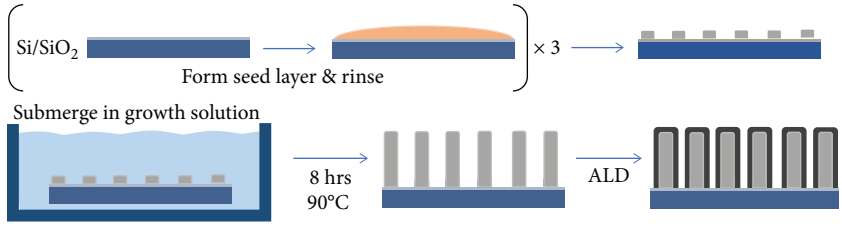

Figure 2: A hybrid ALD/hydrothermal process is used to fabricate the TiO_2@ZnO nanowires. ZnO nanowires are grown hydrothermally. First, a quantum dot seed layer is formed on the surface of an oxidized silicon wafer. The seed layer forms the basis upon which the nanowires grow. Next, the wafer is submerged into Zn-rich growth solution for 8 hours at 250°F; nanowire height can be tuned via growth time. Finally, the ZnO nanowires are coated with TiO_2 using ALD.

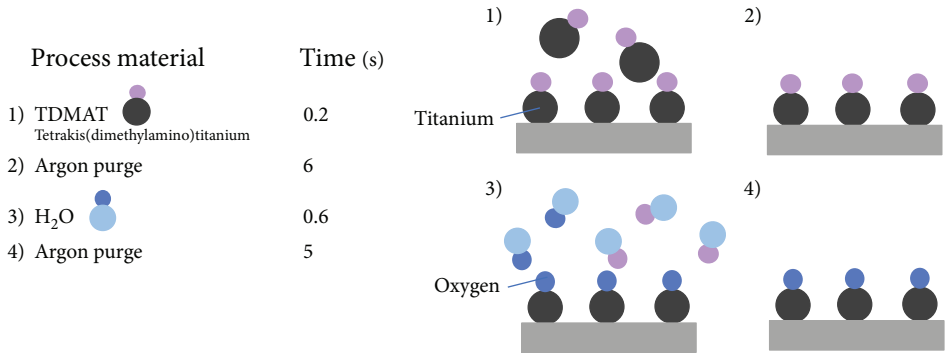

Figure 3: Process flow for ALD TiO_2. TDMAT is adsorbed onto a substrate and the excess purged by argon. Next, H_2O enters the chamber and reacts with TDMAT in a self-limiting reaction; the excess H_2O and by-products are purged by argon.

shown in Figure 3. ALD, a highly precise chemical vapor deposition method, creates uniform, conformal coverage of polycrystalline TiO_2 using a self-limiting reaction. To deposit TiO_2, tetrakis(dimethylamido)titanium (TDMAT) was introduced into the deposition chamber through an argon carrier gas and allowed to adsorb onto the substrate surface for 0.6 s. Excess (unadsorbed) TDMAT was removed from the chamber with argon gas for 5 s. Next, H_2O was introduced for 0.25 s, beginning a self-limiting reaction with adsorbed TDMAT. The excess H_2O and reaction by-products were removed with argon gas for 5 s, leaving a single layer of TiO_2. In this way, gaseous precursors were introduced in a systematic and cyclic manner to create a self-limiting reaction—one layer of TiO_2 was deposited per cycle. This makes ALD an ideal deposition method for high-quality, Ångström-level precision over very high-aspect ratio substrates. The ZnO nanowire array was coated by 1000 cycles of thermally grown ALD TiO_2 (~0.4 Å/cycle) at a process temperature of 250°C, as reported in a previous work [19].

Electrical contact is established using copper tape and insulated tin wire. To isolate the active material, electrodes were passivated onto a glass substrate using epoxy (Figure 4(a)). Photoelectrochemical water splitting was tested using a 3-electrode set-up in 0.5 M H_2SO_4 solution vs. Ag/AgCl with a platinum wire as the counter electrode. An Asahi MAX-303 Xenon lamp was used as the solar simulator and the system was enclosed in TB4 Thorlabs black-out hardboard (5 mm thick with foam core). Electrochemical measurements were conducted using a Gamry Ref. 600 potentiostat (Figure 4(b)). Linear sweep voltammetry was conducted from 0 V vs. Ag/AgCl to 1 V vs. Ag/AgCl, since the aqueous solution had an electrochemical voltage limit of 1.2 V (standard electrode potential of 1.23 V for the $O_2 + 4H^+ + 4e^- \longrightarrow 2H_2O$ reaction). The scans were conducted in dark conditions (covered in a black-out cardboard housing) and light conditions, as well as chopped light––dark alternating with light.

2.1. Cell Efficiency. The ultimate efficiency of a cell (adapted from Hisatomi et al.) [20] can be described by the following equations. First, the solar-to-hydrogen efficiency is

$$\mathrm{STH} = \frac{\text{Representative } H_2 \text{ output energy}}{\text{Energy of incident solar light}} = \frac{r_{H_2} \times \Delta G}{P_{\text{sun}} \times S}, \quad (1)$$

where r_{H_2} is the rate of hydrogen production, ΔG is the change in Gibbs energy, P_{sun} is the energy flux of irradiation, and S is the area of the electrode. However, electrodes that require bias voltage in order to produce measurable photocurrent require voltage compensation in order to calculate cell efficiency. Therefore, the applied-bias-compensated solar-to-hydrogen efficiency and half-cell (to be used with a two-electrode cell) is employed:

$$\mathrm{AB-STH} = \frac{|I| \times \eta_F \times (V_{\text{th}} - V_{\text{bias}})}{P_{\text{sun}}}, \quad (2)$$

where I is the photocurrent density, η_F is the faradaic efficiency, V_{th} is the theoretical voltage for water splitting

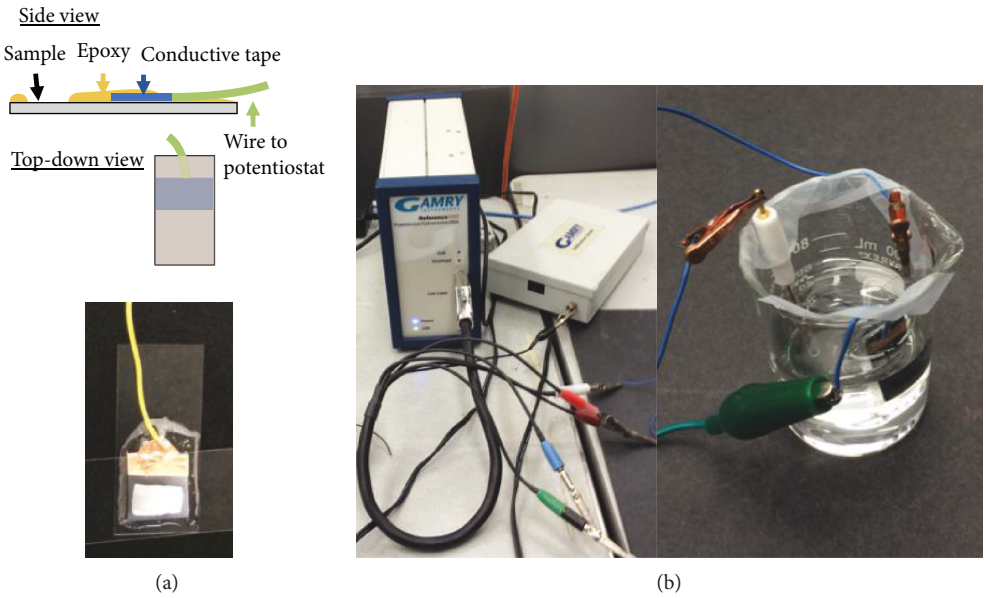

Figure 4: (a) The electrode is prepared for electrochemical testing by passivating the nanowire array onto a glass substrate with epoxy. The active material is isolated with epoxy, and conductive copper tape is used to establish electrical connection. (b) The cell is tested electrochemically using a Gamry Ref. 600 with a 3-electrode setup vs. Ag/AgCl. The counter electrode is platinum.

(1.23 V), and V_{bias} is the applied bias potential. The half-cell STH for a photoanode is therefore

$$\text{HC} - \text{STH} = \frac{|I| \times \left(E_{O_2/H_2O} - E_{\text{RHE}}\right)}{P_{\text{sun}}}, \tag{3}$$

where E_{O_2/H_2O} is the theoretical standard electrode potential for the $O_2 + 4H^+ + 4e^- \longrightarrow 2H\_2\,O$ reaction vs. RHE, and E_{RHE} is the pH-dependent potential of the photoanode in the electrolyte:

$$E_{\text{RHE}} = E_{\text{measured}} - E^0_{\text{Ag-AgCl}} + \frac{RT \ln 10}{F}\text{pH}, \tag{4}$$

where E_{measured} and $E^0_{\text{Ag-AgCl}}$ are the potential measured relative to an Ag/AgCl reference electrode and the standard potential of the Ag/AgCl reaction, respectively. R, T, and F are the gas constant, temperature, and Faraday constant, respectively. Therefore, the cell efficiency is dependent not only on the measured photocurrent density but also on the applied bias potential. Furthermore, texturization, catalysts, and coelectrodes to promote charge separation have been readily shown as methods to increase photocurrent, while fewer work exists on methods to decrease onset voltage, aside from material choices.

3. Results and Discussion

3.1. Characterization. The phase structure of hydrothermally grown ZnO nanowires was characterized using powder X-ray diffraction (XRD). Figure 5 displays the X-ray diffraction peaks, which confirm excellent crystallinity and hexagonal wurtzite ZnO phase (JCPDS card No. 36-1451). The surface

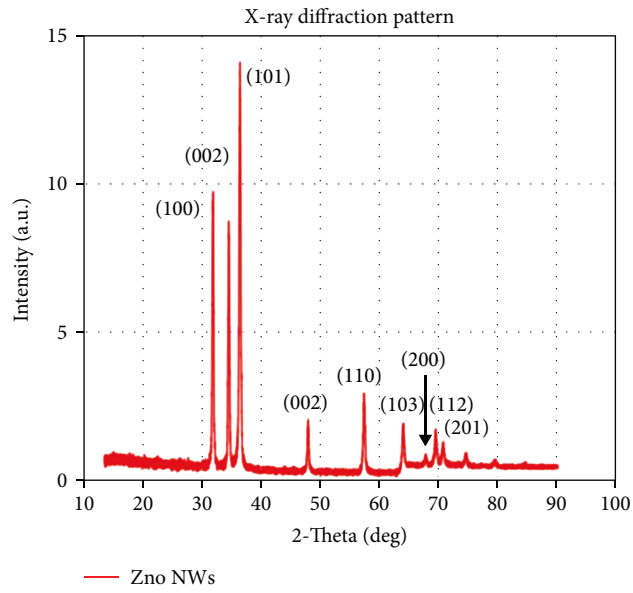

Figure 5: X-ray diffraction pattern of ZnO nanowires, confirming both elemental composition and high crystallinity.

morphology of the nanowire array was analyzed using a field emission scanning electron microscopy (FESEM). SEM images before ALD processing show highly ordered, 10 μm-tall nanowires with diameters of less than 50 nm. Furthermore, the nanowires show polygonal cross sections, implying single-crystalline nature (Figures 6(a), 6(d), and 6(g)). SEM images of the nanowire array post-ALD show complete coverage of TiO_2. As shown in Figures 6(a) and 6(b), a single ZnO nanowire is uniformly coated by TiO_2 when coated at 1000 ALD cycles (Figures 6(c), 6(f), and

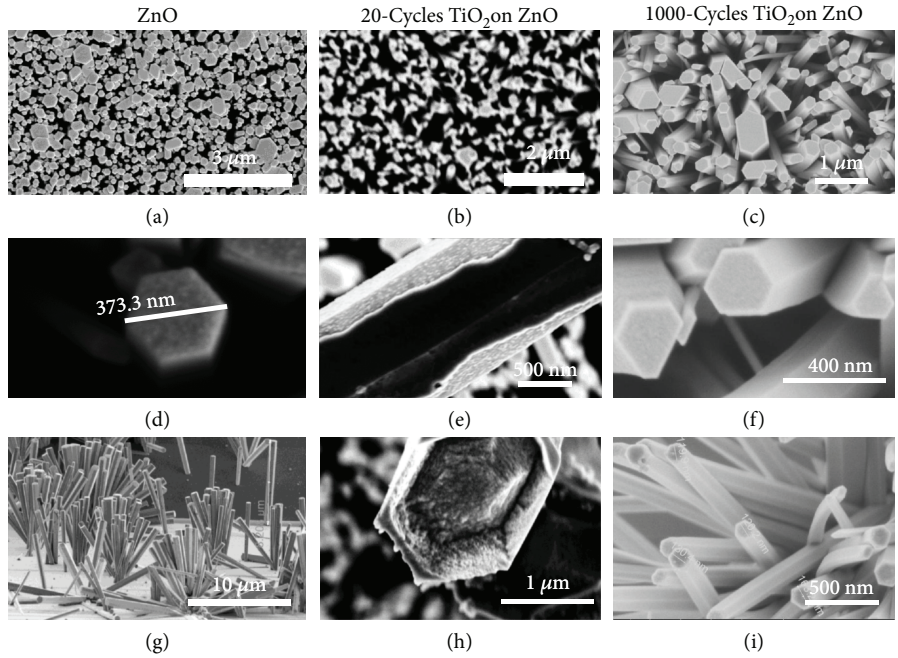

Figure 6: SEM images of ZnO, 20 cycles TiO_2@ZnO (incomplete coverage), and 1000 cycles TiO_2@ ZnO (complete and conformal coverage). (a) Top-down view of ZnO nanowire forest, (b) top-down view of 20-cycle TiO_2-coated ZnO nanowire forest, (c) top-down view of 1000-cycle TiO_2-coated ZnO nanowire forest, (d) single nanowire view of ZnO, showing hexagonal shape (single-crystalline), (e) single nanowire view of 20-cycle TiO_2 on ZnO, showing incomplete coverage, (f) conformally and fully coated 1000-cycle TiO_2@ZnO, (g) side view of ZnO nanowires, (h) side view of 20 cycles TiO_2@ZnO, and (j) side view of 1000 cycles TiO_2@ZnO.

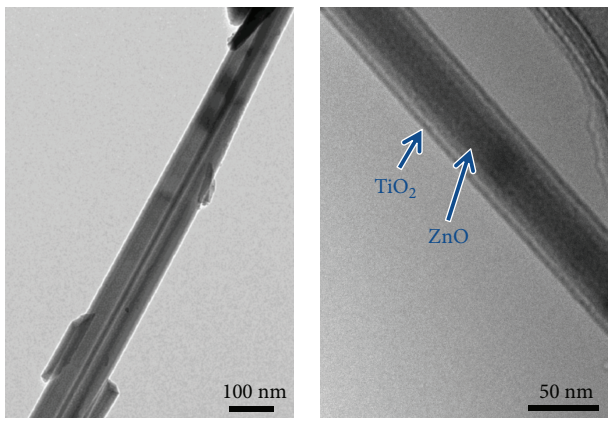

Figure 7: (a) TEM image of a lone ZnO nanowire, with hexagonal shape. (b) TEM image of a 1000-cycle TiO_2@ZnO nanowire, showing conformal coverage along the body of the nanowire.

6(j)), as opposed to 20-cycle coatings of TiO_2, which shows incomplete coverage (Figures 6(b), 6(e), and 6(h)). A transmission electron microscopy (TEM) was employed for the characterization of the single nanowire. Figure 7(a) exhibits a single ZnO nanowire with a hexagonal cross section. Figure 7(b) shows complete and conformal coverage of 1000-cycle TiO_2 on ZnO nanowires. In contrast to previous work on TiO_2, we are able to achieve tall, highly ordered ZnO_2/TiO_2 arrays. By using ALD to deposit a thin coating of TiO_2, we have further limited the distance of travel for minority carriers, minimizing recombination and ensuring better charge separation. The favorable geometry and high-quality coating with ALD allows us to achieve stable devices with excellent-onset voltage, producing photocurrent at extremely low bias voltage.

3.2. Electrochemical Performance. As shown in Figure 8, the ALD TiO_2 shows significant differences in current outputs between light and dark conditions, implying photocurrent under lit conditions, with photocurrent increasing with increasing voltage. While the signal-to-noise is poor due to the low photocurrent, Figure 8 also shows that photocurrent is generated even at very low voltages (low onset voltage). The planar structure made of 1000-cycle TiO_2 coatings shows only marginal improvement in photocurrent over that of 20-cycle TiO_2 (Figures 8(a) and 8(b)) structure; in comparison, texturized TiO_2 as shown in Figure 8(c) shows significantly increased photocurrent. For example, at 0 V vs. Ag/AgCl, 1000-cycle TiO_2 shows an order of magnitude more photocurrent than 20-cycle TiO_2. Furthermore, it is noted that the electrode performances in these tests are in the absence of surface catalysts, which have been shown to greatly increase detectable photocurrent.

As seen in Figure 9(a), the PEC response of the bare ZnO nanoarray is mostly obscured by side reactions, despite cleaning the ZnO with ethanol and DI water. The side reactions cause peaking and sharp increases in current. However, when coated with ALD TiO_2, the electrode is significantly more stable, showing a marked lack of reactions that obscure photocurrent response of the bare ZnO (Figure 9(b)). The results suggest that the hydrothermal growth method for

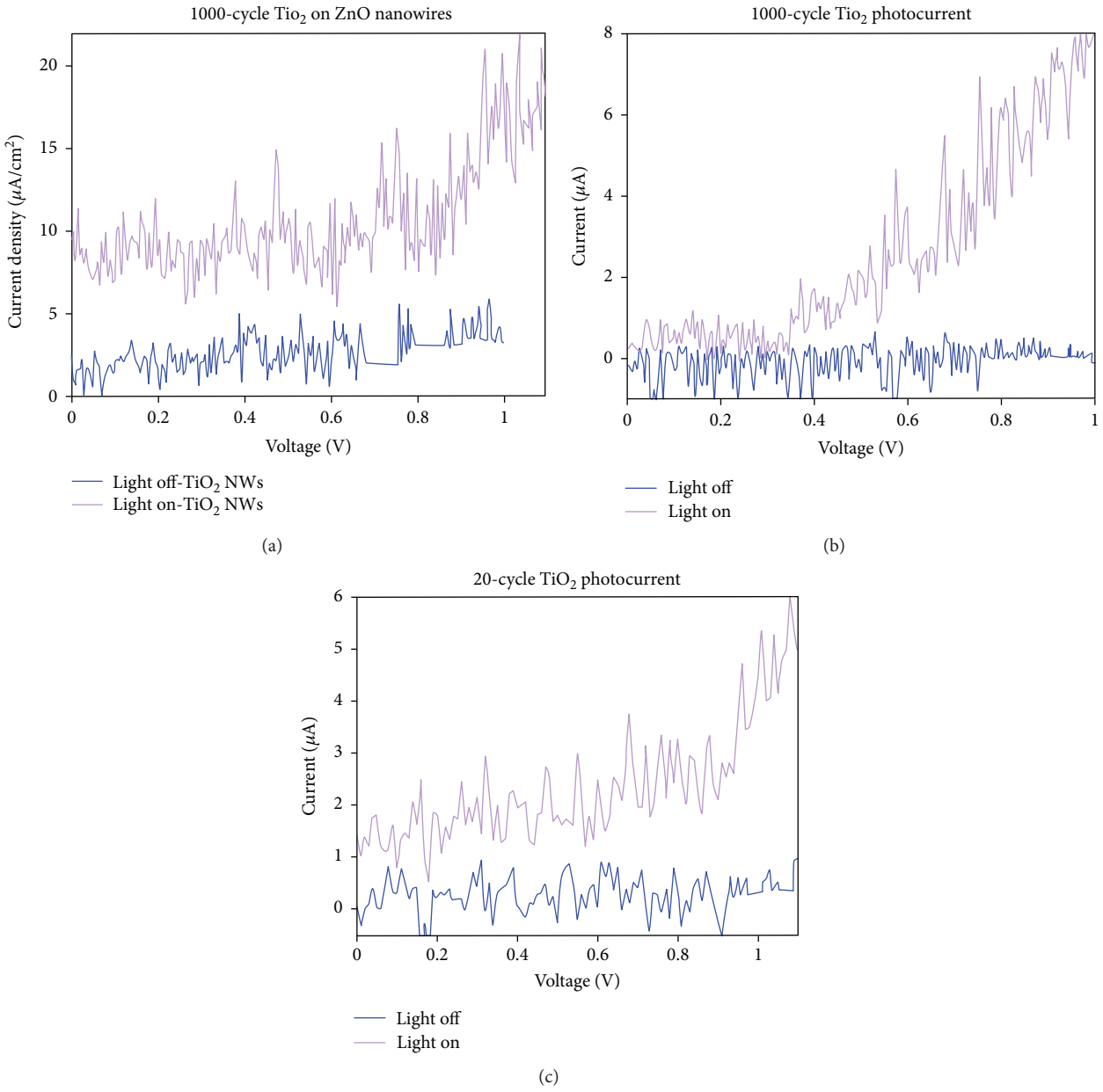

Figure 8: Linear sweep voltammetry under lit and dark conditions. (a) High-aspect ratio TiO_2@ZnO show significantly increased photocurrent (~1 order of magnitude over planar TiO_2 at 0 V vs. Ag/AgCl). (b) Planar 1000 cycle TiO_2 on silicon shows photocurrent ranging from ~0 to 8 μA. (c) Planar 20 cycle TiO_2 on silicon shows photoresponse, with photocurrent ranging from ~1 to 5 μA.

ZnO results in impurities and instabilities that make the ZnO nanowire array unsuitable for photocatalytic water splitting. However, these instabilities are not observed in the ALD TiO_2-coated samples, implying that TiO_2 is capable of stabilization of a ZnO nanowire system as demonstrated in a previous work [21].

Since the grain boundaries of ALD TiO_2 are potential recombination sites, ALD TiO_2 is susceptible to low performance as a PEC electrode. In contrast, the ZnO nanowires are single-crystalline and less vulnerable to recombination sites. By limiting the TiO_2 to a 40 nm coating on the ZnO nanowire, the travel distance of minority carriers to a single-crystalline substrate is greatly reduced, promoting conductivity and reducing recombination. Since the band gap of ZnO relative to TiO_2 is smaller, the generated photoelectrons in TiO_2 should not experience build-up and subsequent recombination at the semiconductor junction.

4. Conclusion

High-aspect ratio and vertically ordered ZnO/TiO_2 nanoarrays as long as 10 μm and less than 50 nm in diameter were successfully synthesized for applications in solar-powered hydrogen (H_2) gas harvesters. Hybrid hydrothermal/ALD processing was used to achieve high-aspect ratio and high-quality nanowire arrays. Surface morphology and phase

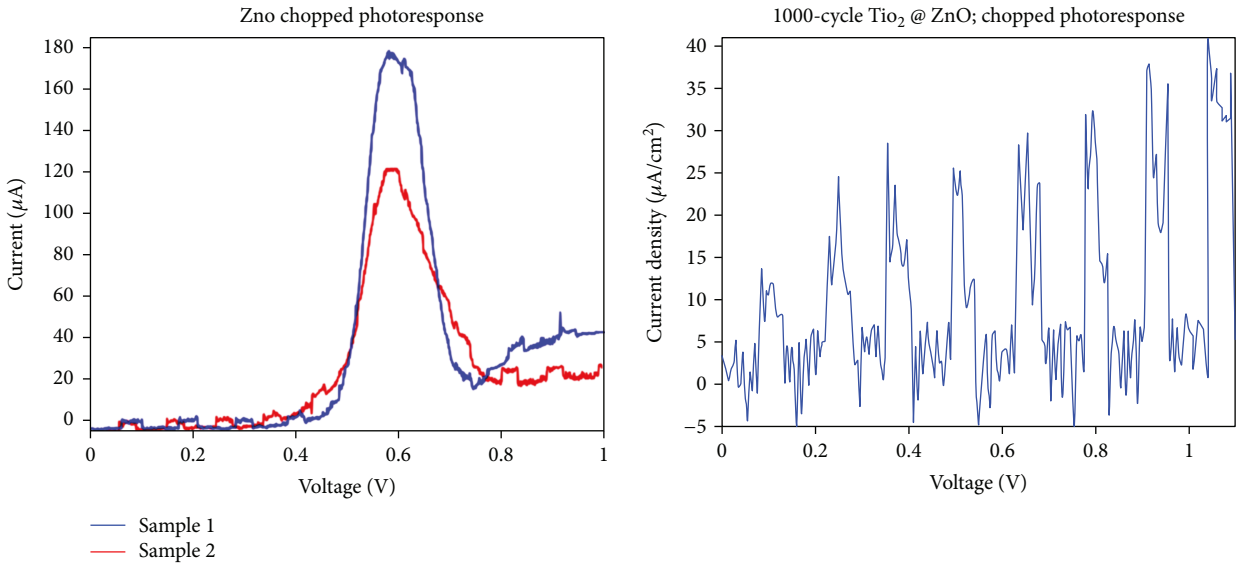

Figure 9: Chopped scans (alternating dark and lit conditions) for (a) bare ZnO nanowires. As can be seen by the linear sweep, hydrothermally grown ZnO nanowires exhibit undesirable side reactions, which obscure photocurrent and compromise stability of the device. In contrast, (b) 1000-cycle TiO_2 shows no such reactions and significant difference between on/off conditions.

structure were analyzed to confirm TiO_2-coated ZnO nanowires. Photoelectrochemical responses of synthesized nanowires were measured to investigate their performance as hydrogen gas harvesters. Nanowires with TiO_2 demonstrated improved stability over bare ZnO nanowires during photocatalysis with low bias voltage. Results show that favorable geometry and high-quality nanowires not only enhanced chemical stability but also improved required bias voltage to yield photocurrent.

Data Availability

The data used to support the findings of this study are available from the corresponding author upon request.

Disclosure

This manuscript is based on the IEEE MEMS 2017 conference paper with the addition of (1) investigation into number of cycles on coverage of the ZnO core with corresponding characterization; (2) LSV under dark and lit conditions, indicating low-onset voltage; (3) performance comparison of planar and texturized, low- and high-cycle number ALD; and (4) band analysis of ZnO-TiO_2 core shell, indicating favorable band structure for water splitting.

Conflicts of Interest

The authors declare that they have no conflicts of interest.

Authors' Contributions

Emmeline Kao and Hyun Sung Park are co-first authors, and contributed equally to this work.

Acknowledgments

This work was performed in part at the Marvell Nanofabrication Laboratory at University of California, Berkeley, and supported in part by Berkeley Sensor and Actuator Center, an NSF/Industry/University Research Collaboration Center. This material is based upon work supported by the National Science Foundation GRFP under Grant No. 1106400. The authors would like to thank Dr. Jinwoo Bae for valuable discussion.

References

[1] G. Conzelmann, M. Petri, C. Forsberg, and B. Yildiz, "Configuration and technology implications of potential nuclear hydrogen system applications," 2005.

[2] Department of Energy, "Hydrogen Production: Biomass-Derived Liquid Reforming," http://energy.gov/eere/fuelcells/hydrogen-production-biomass-derived-liquid-reforming.

[3] Z. Zou, J. Ye, K. Sayama, and H. Arakawa, "Direct splitting of water under visible light irradiation with an oxide semiconductor photocatalyst," *Nature*, vol. 414, no. 6864, pp. 625–627, 2001.

[4] Y. Lin, G. Yuan, R. Liu, S. Zhou, S. W. Sheehan, and D. Wang, "Semiconductor nanostructure-based photoelectrochemical water splitting: a brief review," *Chemical Physics Letters*, vol. 507, no. 4-6, pp. 209–215, 2011.

[5] O. Khaselev and J. A. Turner, "Sex and science," *Science*, vol. 280, no. 5362, pp. 367b–3367, 1998.

[6] T. Bak, J. Nowotny, M. Rekas, and C. Sorell, "Photo-electrochemical hydrogen generation from water using solar energy. Materials-related aspects," *International Journal of Hydrogen Energy*, vol. 27, no. 10, pp. 991–1022, 2002.

[7] G. Mor, K. Shankar, M. Paulose, O. Varghese, and C. Grimes, "Enhanced photocleavage of water using titania

nanotube arrays," *Nano Letters*, vol. 5, no. 1, pp. 191–195, 2005.

[8] N. Meng, M. Leung, D. Leung, and K. Sumathy, "A review and recent developments in photocatalytic water-splitting using TiO_2 for hydrogen production," *Renewable and Sustainable Energy Reviews*, vol. 11, no. 3, pp. 401–425, 2007.

[9] A. Paracchino, V. Laporte, K. Sivula, M. Gratzel, and E. Thimsen, "Highly active oxide photocathode for photoelectrochemical water reduction," *Nature Materials*, vol. 10, no. 6, pp. 456–461, 2011.

[10] C. Liu, J. Tang, H. M. Chen, B. Liu, and P. Yang, "A fully integrated nanosystem of semiconductor nanowires for direct solar water splitting," *Nano Letters*, vol. 13, no. 6, pp. 2989–2992, 2013.

[11] P. Krogstrup, H. I. Jørgensen, M. Heiss et al., "Single-nanowire solar cells beyond the Shockley–Queisser limit," *Nature Photonics*, vol. 7, no. 4, pp. 306–310, 2013.

[12] R. van de Krol and M. Grätzel, "Photoelectrochemical hydrogen production," in *Electronic Materials: Science & Technology*, Springer, Boston, MA, USA, 2012.

[13] A. Fujishima and K. Honda, "Electrochemical photolysis of water at a semiconductor electrode," *Nature*, vol. 238, no. 5358, pp. 37-38, 1972.

[14] M. Weber and M. Dignam, "Splitting water with semiconducting photoelectrodes—efficiency considerations," *International Journal of Hydrogen Energy*, vol. 11, no. 4, pp. 225–232, 1986.

[15] A. Fujishima, T. N. Rao, and D. A. Tryk, "Titanium dioxide photocatalysis," *Journal of Photochemistry and Photobiology C: Photochemistry Reviews*, vol. 1, no. 1, pp. 1–21, 2000.

[16] S. N. Frank and A. J. Bard, "Heterogeneous photocatalytic oxidation of cyanide ion in aqueous solutions at titanium dioxide powder," *Journal of the American Chemical Society*, vol. 99, no. 1, pp. 303-304, 1977.

[17] J. H. Park, O. O. Park, and S. Kim, "Photoelectrochemical water splitting at titanium dioxide nanotubes coated with tungsten trioxide," *Applied Physics Letters*, vol. 89, no. 16, p. 163106, 2006.

[18] J. Bolton, S. Strickler, and J. Connolly, "Limiting and realizable efficiencies of solar photolysis of water," *Nature*, vol. 316, no. 6028, pp. 495–500, 1985.

[19] H. S. Park, E. Kao, X. Zang, and L. Lin, "High aspect ratio-titanium dioxide-stabilized zinc oxide nanowires for photocatalytic hydrogen gas harvester," in *2017 IEEE 30th International Conference on Micro Electro Mechanical Systems (MEMS)*, pp. 667–670, Las Vegas, NV, USA, 2017.

[20] T. Hisatomi, J. Kubota, and K. Domen, "Recent advances in semiconductors for photocatalytic and photoelectrochemical water splitting," *Chemical Society Reviews*, vol. 43, no. 22, pp. 7520–7535, 2014.

[21] M. Liu, C. Y. Nam, C. T. Black, J. Kamcev, and L. Zhang, "Enhancing water splitting activity and chemical stability of zinc oxide nanowire photoanodes with ultrathin titania shells," *The Journal of Physical Chemistry C*, vol. 117, no. 26, pp. 13396–13402, 2013.

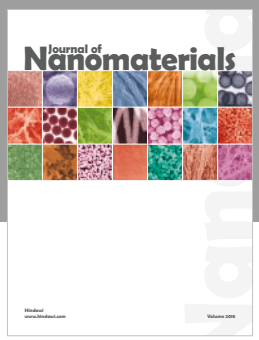

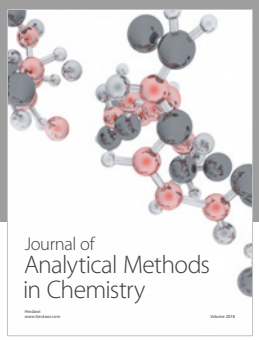

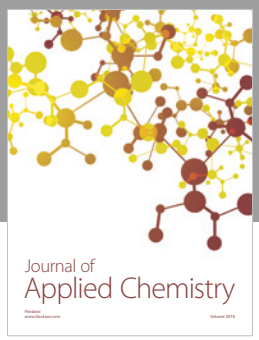

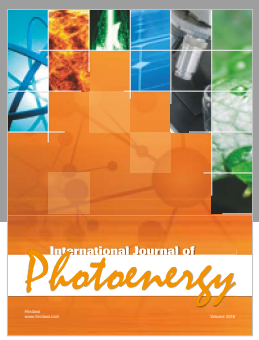

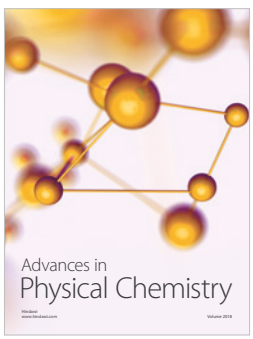

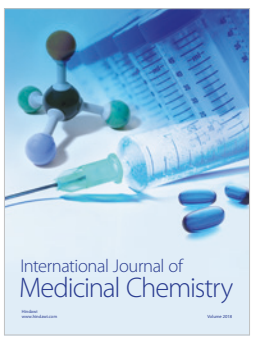

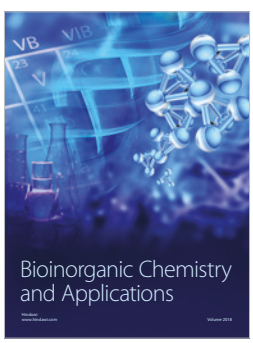

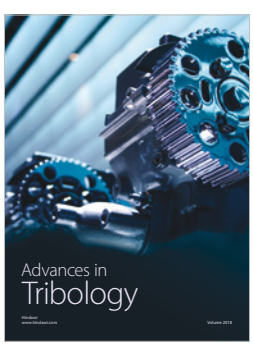

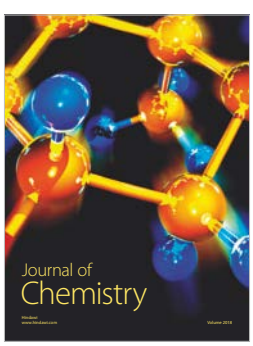

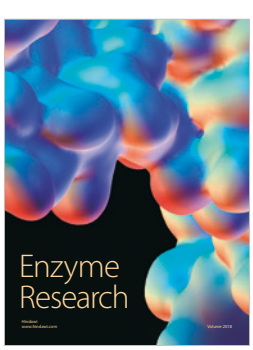

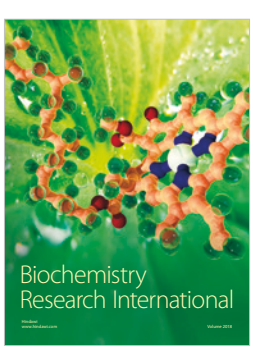

Hindawi

Submit your manuscripts at
www.hindawi.com